Letter | Editors' Suggestion

Non-Fermi liquid transport and strong mass enhancement near the nematic quantum critical point in $FeSe_xTe_{1-x}$ thin films

Yuki Sato [1,*] Soma Nagahama [2] Ilya Belopolski [1] Ryutaro Yoshimi [1,3] Minoru Kawamura [1] Atsushi Tsukazaki [2,4] Akiyoshi Yamada [1,5] Masashi Tokunaga [1,5] Naoya Kanazawa [6] Kei S. Takahashi [1] Yoshichika Ōnuki [1] Masashi Kawasaki [1,2] and Yoshinori Tokura [1,2,7]

[1] *RIKEN Center for Emergent Matter Science (CEMS), Wako 351-0198, Japan*

[2] *Department of Applied Physics and Quantum-phase Electronics Center (QPEC), University of Tokyo, Tokyo 113-8656, Japan*

[3] *Department of Advanced Materials Science, University of Tokyo, Kashiwa 277-8561, Japan*

[4] *Institute for Materials Research (IMR), Tohoku University, Sendai 980-8577, Japan*

[5] *Institute for Solid State Physics, University of Tokyo, Kashiwa 277-8581, Japan*

[6] *Institute of Industrial Science, University of Tokyo, Tokyo 153-8505, Japan*

[7] *Tokyo College, University of Tokyo, Tokyo 113-8656, Japan*

(Received 22 December 2024; revised 17 June 2025; accepted 27 June 2025; published 22 July 2025)

Unconventional superconductivity is often accompanied by non-Fermi liquid (NFL) behavior, which emerges near a quantum critical point (QCP)— a point where an electronic ordered phase is terminated at absolute zero under nonthermal parameters. While nematic orders, characterized by broken rotational symmetry, are sometimes found in unconventional superconductors, the role of nematic fluctuations in driving NFL transport behavior remains unclear. Here, we investigated electrical and thermoelectric transport properties in $FeSe_xTe_{1-x}$ thin films and observed hallmark NFL behavior: temperature-linear resistivity and logarithmic divergence of thermoelectricity at low temperatures. Notably, the thermoelectricity peaks sharply at the nematic QCP ($x = 0.45$), highlighting the dominant role of nematic fluctuations in the NFL transport. Furthermore, we found that the pair-breaking mechanisms in the superconducting phase crosses over from orbital- to Pauli-limited effects, indicating the mass enhancement near the nematic critical regime. These findings reveal the profound impact of nematic fluctuations on both normal-state transport and superconducting properties.

DOI: 10.1103/8zfz-252m

One of the central challenges in researching unconventional superconductivity is understanding the role of quantum fluctuations in non-Fermi liquid (NFL) transport near a quantum critical point (QCP), where a second-order phase transition takes place at absolute zero [1–4]. In some strongly correlated superconductors, such as cuprate [5], iron-based superconductors [6], layered kagome superconductor [7], and magic-angle twisted bilayer graphene [8], an electronic nematic state has been observed, where the electronic system breaks the rotational symmetry while preserving the underlying lattice translational symmetry. Investigating transport properties near a QCP associated with such nematic orders is of great importance, as it may be linked to the symmetry of the superconducting order parameter and the microscopic pairing mechanisms. In the vicinity of a QCP, strong renormalization of quasiparticle mass m^* has been reported [2,9], attributed to enhanced electron correlations by quantum fluctuations. However, because nematic orders often coexist or compete with other electronic orderings such as magnetism and charge-density waves, accessing a pure nematic QCP, isolated from the other order, poses a significant challenge. Consequently, it remains unclear whether nematic fluctuations alone are responsible for the observed NFL transport behavior and mass enhancement in strongly correlated superconductors.

Iron-chalcogenide superconductors have attracted considerable attention due to their unique electronic properties owing to the strongest electronic correlations among the iron-based superconductor family [10–12]. FeSe stands out in this family for exhibiting an electronic nematic phase in the absence of magnetism. Isovalent substitution of Se with Te in a form of $FeSe_xTe_{1-x}$ (FST) significantly alters its electronic structure in several ways. First, it monotonically suppresses the nematic order, with the transition temperature T_{nem} reaching absolute zero around $x = 0.45$, leading to a nematic QCP [13] [Fig. 1(a)]. Correspondingly, nematic susceptibility shows a pronounced divergence around $x = 0.5$ [14,15]. Second, Te substitution enhances the interlayer Te5p_z -5 p_z hybridization owing to a large ionic radius of Te compared to Se, and reduces the intralayer hopping within the iron-chalcogenide plane. This leads to the enhancement of electronic correlations within the layer [11,12]. In the end compound FeTe, a double-stripe antiferromagnetic (AFM) state emerges with an ordering vector $Q = (\pi, \pi)$ below Néel temperature $T_N \sim 75$ K [16]. This AFM phase is steeply suppressed as Te content decreases, resulting in another potential QCP associated with the disappearance of AFM order around $x = 0.08$ [17] [Fig. 1(a)].

The quantum criticality associated with the disappearance of nematic order has been studied in an analogous compound Fe(Se,S) (FSS). Near the nematic QCP in FSS, thermoelectric measurements have revealed strong electronic

*Contact author: yuki.sato.yj@riken.jp

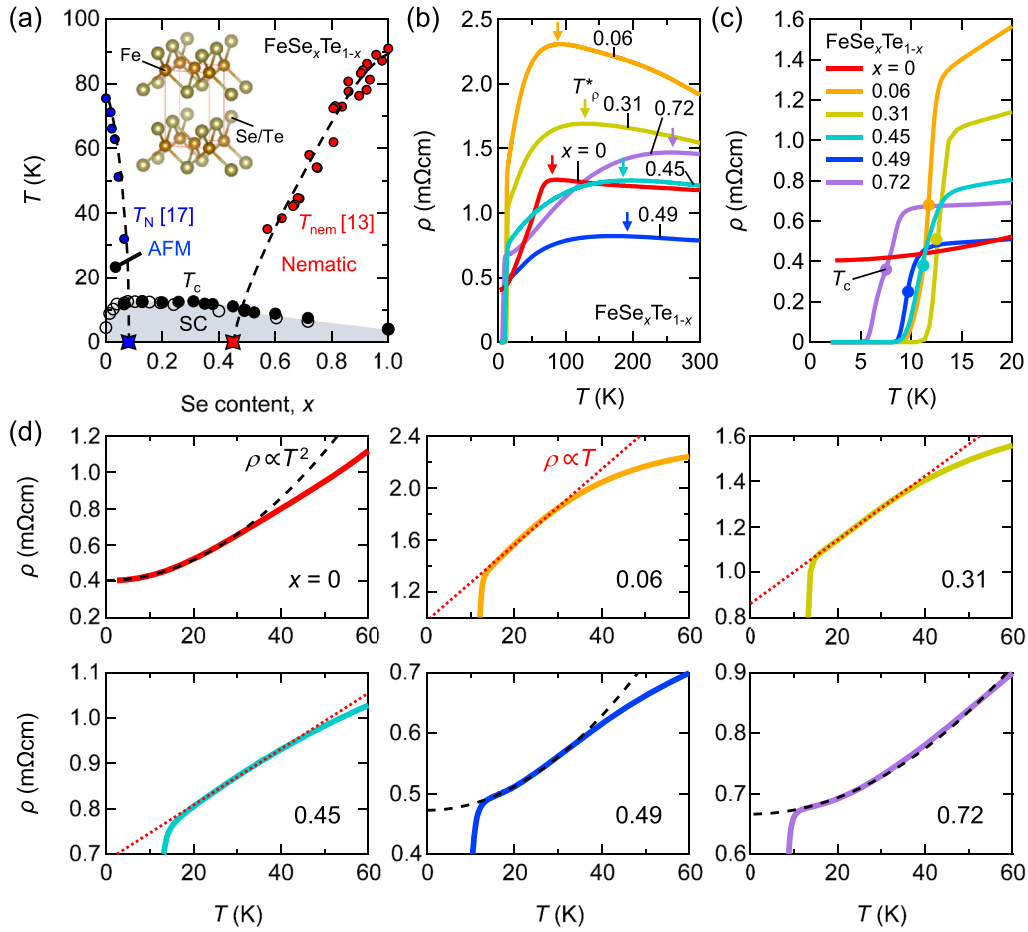

FIG. 1. Non-Fermi liquid (NFL) transport signature in FST thin films. (a) T-x phase diagram of $FeSe_xTe_{1-x}$ (FST). The black and white markers represent T_c for FST thin films grown on STO and CdTe substrates [27], respectively. The red and blue markers, respectively, denote T_{nem} [13] and T_N [17], adopted from resistivity measurements on bulk single crystals. The inset shows the crystal structure of FST in the tetragonal phase [28]. (b) ρ-T curves for FST thin films with various x ranging from 0 to 0.72. Arrows indicate T_ρ^*, where ρ reaches its maximum. (c) Low-temperature expansion of (b). Markers denote T_c for each sample. (d) Low-temperature normal state resistivity below 60 K. Red dashed lines show linear fits ($\rho_0 + A_1 T$), while black dashed lines represent quadratic fits ($\rho_0 + A_2 T^2$) in the low-temperature region above T_c.

correlations [18], while high magnetic field transport measurements revealed temperature (T)-linear resistivity [19], suggesting a connection between nematic fluctuations and NFL transport. However, there are concerns regarding FSS as a system hosting a pure nematic QCP. First, S substitution induces a Lifshitz transition near, but not exactly at, the nematic QCP [20]. This introduces an additional change in thermoelectricity, making it difficult to isolate the quantum critical response in FSS. Second, nuclear magnetic resonance (NMR) experiments have reported significant AFM fluctuations near the nematic QCP of FSS [21]. In contrast, NMR studies on FST reveal a nearly T-independent spin-lattice relaxation rate at $x = 0.42$, suggesting the absence of significant AFM fluctuations around the nematic QCP [22]. Accordingly, the nematic QCP in FST is isolated from the AFM fluctuations, making FST an ideal materials platform for studying the intrinsic physics associated with this pure nematic QCP. To date, it remains unclear whether nematic fluctuations alone can induce mass enhancement at the pure nematic QCP [20,23,24].

One of the challenges in studying the systematic transport properties of FST is synthesis of high-quality homogeneous crystals across the entire x range. Earlier studies on thermoelectricity in FST have focused on bulk single crystals [25]. However, solid-state reaction methods result in phase separation within a certain composition range ($0.6 \leqslant x \leqslant 0.9$), while the chemical vapor transport technique can produce high-quality single crystals, but only for Se-rich compositions ($0.5 \leqslant x \leqslant 1$) [13], preventing the investigation of transport properties in the wide x range. Additionally, one has to carefully treat them with annealing procedure, which is believed to remove excess interstitial Fe atoms and enhances superconductivity [26]. In contrast, the molecular beam epitaxy (MBE) technique enables the fabrication of FST thin films across the entire x range without phase separation [27]. MBE also offers a controllable *in situ* Te-annealing and capping process, which is useful in preserving modest superconductivity [27]. Practically, MBE allows relatively short fabrication time (several hours per composition) compared to that typically required for bulk crystal growth, enabling the production and

characterization of dozens of films in this study. Given these advances in sample growth techniques, it is meaningful to revisit the thermoelectric properties of FST grown by state-of-the-art MBE techniques, particularly around the nematic QCP, to probe the intrinsic transport properties driven by nematic fluctuations (see Supplemental Material [29] and Refs. [30–32] therein, for discussion about nematic transition in FST thin films).

In this Letter, we present an experimental study of electrical resistivity ρ, Seebeck coefficient S, and upper critical field H_{c2} for MBE-grown FST thin films spanning a wide range of x across the nematic QCP. We observe hallmark NFL transport behavior in both resistivity and Seebeck coefficient: T-linear resistivity and a logarithmic divergence of Seebeck coefficient, $S/T \propto \ln T$, near the nematic QCP at $x = 0.45$. These results support the scenario in which nematic fluctuations drive NFL transport behavior in strongly correlated metals. Additionally, we observe a crossover in the dominant pair-breaking mechanisms from orbital to Pauli effect around the nematic QCP, indicative of a mass enhancement due to nematic quantum criticality. Our results thus point to the strong connection between nematic fluctuations and NFL transport properties and their impact on superconducting pair-breaking mechanisms.

We investigate the electrical resistivity ρ of FST films with a wide composition range of $0 \leqslant x \leqslant 0.72$, as a function of T [Fig. 1(b)]. As T decreases, ρ increases at high temperatures, peaks at temperatures T_ρ^* [as indicated by the arrows in Fig. 1(b)], turns to decrease with a strong suppression of ρ at low temperatures, and finally drops to zero at the superconducting transition temperature T_c, except for the nonsuperconducting FeTe ($x = 0$) [Fig. 1(c)]. The overall behavior is similar to that of Te-annealed bulk FST crystals with minimal excess iron [26]. This similarity suggests that the content of excess irons is successfully reduced in the MBE-grown FST thin films processed with Te annealing.

Remarkably, the ρ-T curves for the FST thin films can be classified into two categories based on their curvatures at low temperatures: one with T^2 dependence and the other with T-linear dependence. In the former category, including $x = 0$, 0.49, and 0.72, ρ continues to decrease with a downward concavity as T decreases, and it appears to saturate at low temperatures. This behavior is characteristics of Fermi liquid (FL) transport, and the ρ-T curves in this category can be fitted with $\rho = \rho_0 + A_2 T^2$ at sufficiently low temperatures, as shown by the black dashed lines in Fig. 1(d). In the other category, including $x = 0.06$, 0.31, and 0.45, ρ decreases steeply with an upward concavity without saturation down to T_c. The upward concavity corresponds to a low power $n \leqslant 1$ in an empirical model $\rho = \rho_0 + AT^n$, suggesting the absence of FL transport down to T_c. Notably, as shown in the red dashed lines in Fig. 1(d), the ρ-T curves for this category exhibits T-linear resistivity ($\rho = \rho_0 + A_1 T$) at sufficiently low temperatures but above T_c, reminiscent of quantum critical metals near AFM QCPs, such as heavy fermions [1] and cuprates [33]. We note that the value of ρ for all the samples investigated is comparable to or even exceeds the Mott-Ioffe-Regel (MIR) limit of $\rho_{MIR} \sim 0.8$ mΩcm for FST, where the mean free path ℓ becomes extremely short and reaches the lattice constant (see Supplemental Material [29] for more details). This indicates that FST films lie within the *bad metal* regime [4], suggesting that the large value of ρ is not dominated by extrinsic disorder but is likely an intrinsic feature driven by strong quantum fluctuations.

Thermoelectricity is another highly sensitive probe for detecting quantum criticality in the normal state of unconventional superconductors. It is widely acknowledged that the Seebeck coefficient divided by temperature, S/T, remains constant within the framework of FL theory. In contrast, in the NFL regime, S/T can exhibit a logarithmic divergence with approaching an AFM QCP, as given by $S/T \sim A_S \ln T$ [34], where A_S serves as a measure of quantum fluctuations (see Supplemental Material [29] for more details).

Figure 2(a) shows the T dependence of S for the series of FST thin films with various x. The non-T-linear behavior of S across the entire temperature range cannot be explained solely within the framework of the FL theory. To assess the NFL transport properties in the thermoelectricity, we plot S/T as a function of the logarithmic scale of T [Figs. 2(b)–2(g)]. At high temperatures above approximately 100 K, S shows an almost T-independent positive value, except for the negative S in $x = 0$. This behavior is consistent with Heikes formalism, where strong on-site Coulomb interactions lead to T-independent S [35]. Upon decreasing T, S/T begins to decrease at T_S^* [Fig. 2(h)], exhibits a sign change from positive to negative at T_{S0}^*, and shows a logarithmic increase over a temperature range typically spanning 10–50 K, as indicated by the solid lines in Figs. 2(b)–2(g). Further decrease in T results in an abrupt reduction in the amplitude of S/T at T_c due to the superconducting transition, except the nonsuperconducting $x = 0$. Additionally, S/T saturates at low temperatures for $x = 0$ and 0.72 [the dotted lines in Figs. 2(b) and 2(g)], consistent with the formation of FL state, as evidenced by the T^2 dependence of ρ.

The observed logarithmic divergence of S/T in FST thin films [36] is reminiscent of a similar behavior reported in various quantum critical metals near AFM QCPs, including heavy fermions [34], cuprates [37,38], and iron arsenides [35,39]. At AFM QCPs, this logarithmic divergence arises from enhanced scattering processes mediated by spin fluctuations, which leads to T-dependent mass renormalization, $m^*/m \sim \ln(1/T)$ [34]. Such mass enhancement is often evidenced by a strong enhancement of the electronic specific heat near magnetic QCPs [2]. In FST, field dependence of S is very weak, consistent with the earlier work on bulk single crystals [25], suggesting that magnetic contributions to thermoelectricity, such as the magnon-drag effect, are negligible (Fig. S5). Therefore, the logarithmic divergence of S/T near the nematic QCP in FST suggests a strong connection between nematic fluctuations and the observed NFL transport behavior, accompanied by strong mass enhancement [23].

To investigate the impact of nematic quantum criticality on superconducting properties, we measured upper critical fields for superconductivity of FST thin films. We present a set of representative magnetotransport data of H-fixed T scans [Fig. 3(a)] and T-fixed H scans [Fig. 3(b)] for an FST thin film with $x = 0.13$ (see Supplemental Material [29] and Ref. [40] therein). In this study, the magnetic field is applied in the out-of-plane ($H||c$) direction. We define T_c and H_{c2} at the point where $\rho(T, H)$ becomes half of its value in the

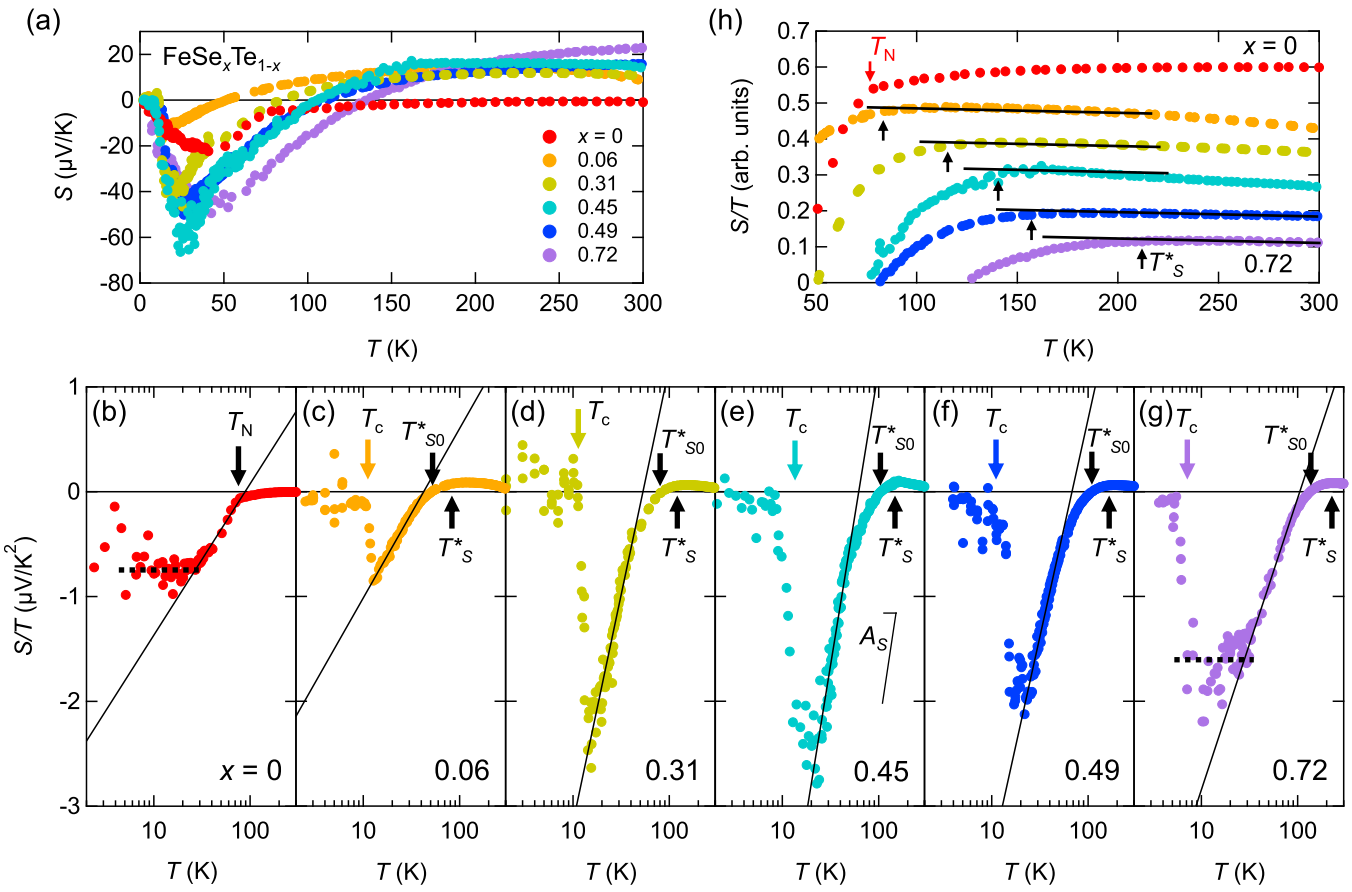

FIG. 2. Thermoelectric signatures of NFL transport behavior in FST thin films. (a) T dependence of S for FST thin films with $x = 0$–0.72. (b)–(g) S/T plotted against logarithmic scale of T for various x. The solid lines represent linear fits indicating logarithmic divergence of S/T, with A_S denoting the slope of the fits. The temperature range for these fittings is (b) 25–80 K, (c) 15–40 K, (d) 15–40 K, (e) 20–50 K, (f) 20–60 K, and (g) 25–95 K, respectively. For $x = 0$ and 0.72, dashed lines show the saturation of S/T. T_c and T_N, determined from ρ-T curves, are also shown. T^*_{S0} is the temperature where $S/T = 0$, while T^*_S is the offset temperature for NFL transport [see (h)]. (h) High-temperature expansion of S/T with offsets for clarity. At high temperatures, S/T shows weak dependence on T, as indicated by the black lines. T^*_S is defined as the temperature below which S/T deviates from these lines for $0.06 \leqslant x \leqslant 0.72$. For $x = 0$, S/T exhibits a kink anomaly at T_N.

normal state (50% criterion), as indicated by the arrows in Figs. 3(a) and 3(b). To explore the x-dependent evolution of the pair-breaking mechanism, we constructed H-T phase diagrams from magnetotransport experiments on a series of FST thin films [Fig. 3(c)]. In Se-rich samples, such as $x = 0.72$, H_{c2} exhibits an almost linear increase upon decreasing T, and with a relatively small initial slope at the zero-field critical temperature $T_{c,0}$, $dH/dT|_{T_{c,0}} \sim -4.65$ (T/K). In contrast, in Te-rich compositions such as $x = 0.06$, H_{c2} shows a sharp increase with an upward convex shape near $T_{c,0}$ and with a significantly larger initial slope of $dH/dT|_{T_{c,0}} \sim -15.48$ (T/K).

There are two kinds of pair-breaking effects in a type-II superconductor: the orbital effect and the Pauli paramagnetic effect. The orbital effect is associated with the kinetic energy of the supercurrent around vortices, while the Pauli effect arises from the gain of Zeeman energy by destroying spin-singlet Cooper pairing. There is a notable difference in T dependence of the two critical fields near $T_{c,0}$: $H^{\mathrm{orb.}}_{c2} \propto (T_{c,0} - T)$ for the orbital-limiting upper critical field, while $H^{\mathrm{P}}_{c2} \propto (T_{c,0} - T)^{1/2}$ for the Pauli-limiting upper critical field. The T-linear initial slope for $x = 0.72$ thus suggests a substantial orbital effect, while the T-sublinear dependence for $x = 0.06$ indicates a dominant Pauli effect.

To clearly visualize the quantum critical region in the phase diagram, we constructed a color plot for the power-law exponent n for ρ-T [Fig. 4(a)]. We calculated n as

$$n = \partial \ln(\rho(T) - \rho_0)/\partial \ln T, \tag{1}$$

where residual resistivity ρ_0 is determined by fitting the data using the empirical model $\rho = \rho_0 + AT^n$ at the low-temperature region above T_c (see also Fig. S3). Remarkably, we found that the T-linear resistivity, corresponding $n = 1$, is observed over a wide x range of $0.06 \leqslant x \leqslant 0.45$, which appears to reconcile with the x range where the logarithmic divergence of S/T is observed down to T_c. Intriguingly, as shown in Fig. 4(b), the logarithmic-term prefactor $|A_S|$ shows a pronounced peak notably at the nematic QCP $x = 0.45$, suggesting the dominant role of nematic fluctuations in driving the NFL transport. We consistently observe this feature in zero-temperature intercept of S/T, $|S/T(T \to 0)|$ (see Supplemental Material [29] and Ref. [41] therein). As x decreases, $|A_S|$ exhibits a monotonic decline toward the AFM QCP at

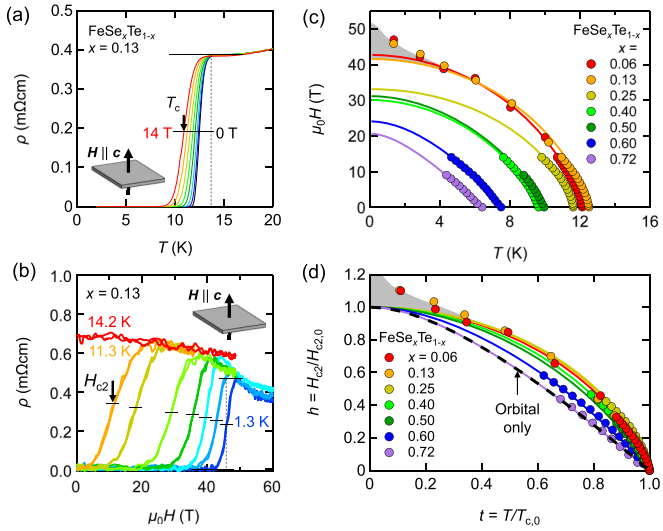

FIG. 3. Crossover of pair-breaking mechanisms from orbital to Pauli effect. (a) ρ-T curves for an FST ($x = 0.13$) thin film under out-of plane magnetic fields, shown in 2 T intervals. T_c is defined as the temperature where ρ becomes half that in the normal state (50% criterion). (b) ρ-H curves at $T =$ 1.3, 2.9, 4.2, 6.0, 8.1, 10.2, 11.3, and 14.2 K. H_{c2} is determined using the 50% criterion. (c) H-T phase diagram for FST with $0.06 \leqslant x \leqslant 0.72$. The solid curves are fits to the WHH formula incorporating the orbital, Pauli, and spin-orbit scattering terms, with λ_{SO} fixed at 1.0. The grey area indicates the region where H_{c2} deviates from the fits, suggesting a possible high-field superconducting phase. (d) Same plot as (c) but plotted against the reduced parameters h and t. The dashed line denotes the WHH formula, incorporating only the orbital effect.

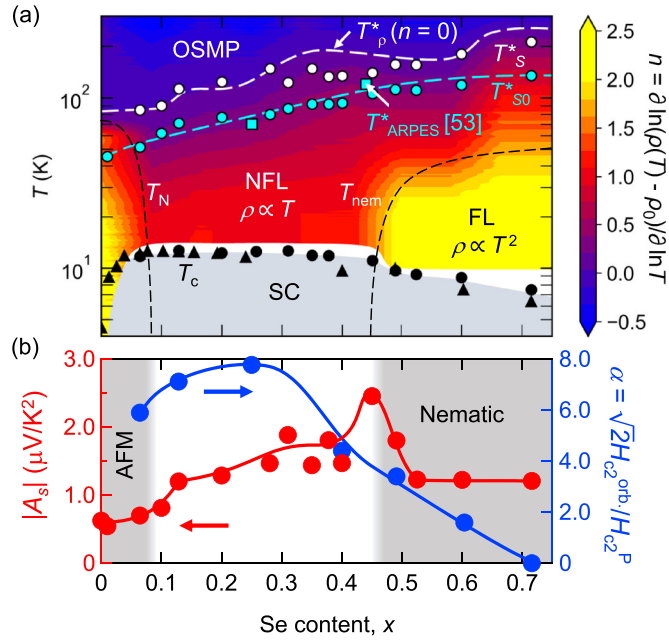

FIG. 4. NFL transport and mass enhancement over the phase diagram. (a) T-x phase diagram with a color plot showing the resistivity power $n = \partial \ln(\rho(T) - \rho_0)/\partial \ln T$. The yellow, red, and blue regions represent Fermi liquid (FL) ($n \sim 2$), non-Fermi liquid (NFL) ($0 < n < 2$), and orbital-selective Mott phase (OSMP) ($n \leqslant 0$), respectively. The white and cyan circles denote T_S^* and T_{S0}^* estimated from the Seebeck coefficient measurements. The cyan squares denote T_{ARPES}^*, below which the Fe $3d_{xy}$ band becomes coherent [53]. The white dashed line represents the $n = 0$ contour where ρ takes its maximum. The cyan dashed line is a guide for the eyes. The black triangles and circles indicate T_c for FST thin films grown on CdTe and STO substrates, respectively. The black dashed lines represent T_N and T_{nem}. (b) x dependence of the logarithmic growth of thermoelectricity, $|A_S|$ (left axis), and the Maki parameter α (right axis). The solid lines are guides for the eyes.

$x = 0.08$ without a peak and is further suppressed within the AFM phase. This result suggests that the AFM QCP could be detrimental to quantum fluctuations, which appears to be consistent with the first-order phase transition in FeTe [16,42] that is, in general, not preferable to enhancing quantum fluctuations.

The NFL behavior gradually fades out at high temperatures above approximately 50 K, and the resistivity turns to decrease ($n < 0$) above around 100 K. Notably, T_S^* estimated from S/T [Fig. 2(h)] closely aligns with T_ρ^*, or identically the contour $n = 0$, indicating a good agreement in the onset temperature below which the NFL behavior begins to develop in both resistivity and thermoelectricity [Fig. 4(a)]. Interestingly, the breakdown of the T-linear resistivity in FST at relatively low temperatures contrasts with the transport properties in cuprates, where T-linear resistivity persists up to 500 K [4]. This behavior in FST rather resembles that observed in heavy fermion systems, where itinerant electrons undergo incoherent scatterings above the Kondo temperatures. The high-temperature insulating behavior in FST might be similarly attributed to incoherent Kondo scatterings with localized Fe $3d_{xy}$ electrons, which stems from the strong Hund coupling (OSMP: orbital-selective Mott phase) [42], reflecting the stronger electronic correlations towards the end composition $x = 0$ (see Supplemental Material [29]) for more details). Angle-resolved photoemission spectroscopy (ARPES) studies have reported that the Fe $3d_{xy}$ orbital forms a large incoherent hole band around the Γ point, which disappears at low temperatures below T_{ARPES}^* [43]. This incoherent hole band naturally explains the T-independent positive S at high temperatures. We find that T_{ARPES}^* is close to T_{S0}^* [Fig. 4(a)], suggesting that the sign change in S/T is linked to the crossover from the high-temperature incoherent OSMP to the low-temperature coherent quantum critical metal.

A further similarity between FST and heavy fermion superconductors lies in their pair-breaking mechanisms. To quantify the dominant pair-breaking effects, it is useful to introduce the ratio of the two upper critical fields, the Maki parameter $\alpha = \sqrt{2}H_{c2}^{orb.}/H_{c2}^{P}$, which becomes larger (smaller) than unity when the Pauli (orbital) effect is dominated. We calculated α by performing fittings with the Werthamer-Helfand-Hohenberg (WHH) formula, incorporating both orbital and Pauli effects [43] (see Supplemental Material [29] for more details). The fitting results are presented as the solid lines in Figs. 3(c) and 3(d). We found that α is negligibly small at $x = 0.72$, but increases with decreasing x, and becomes well above unity in Te-rich FSTs [Fig. 4(b)]. We stress that the large α exceeding unity for the out-of-plane field configuration is extremely rare and reported only in heavy fermion systems [44] and FST with x

around 0.45 [45–47], while it can be easily found for in-plane configurations in various low-dimensional materials [48–52] (see Supplemental Material for in-plane H_{c2} of FST thin films [29]), where the orbital motion perpendicular to magnetic field is quenched due to dimensionality. Remarkably, we found a notable coincidence in the x range ($0.06 \leqslant x \leqslant 0.45$), where α significantly exceeds unity and the NFL transport behavior is observed. This coincidence can be naturally understood in terms of the mass enhancement because α is also related to m^* in the BCS limit [54] as

$$\alpha \approx 2\frac{m^*}{m_0}\frac{\Delta}{E_F}, \tag{2}$$

where m_0 is the bare electron mass, Δ is superconducting gap, and E_F is Fermi energy. Indeed, a large α exceeding unity in heavy fermions is predominantly driven by the strong mass renormalization via Kondo effect [44]. Our results thus suggest a close link between the unusually Pauli-limited H_{c2} and the nematic quantum criticality in FST.

We note that the WHH fittings reasonably capture all the H_{c2} data except for the low-temperature regime in $x = 0.06$ and 0.13, where deviations from the fitting are observed as slight upturns in H_{c2}, indicated by the shaded areas in Figs. 3(c) and 3(d). As sufficiently large α (>1.5) is one of the requisites for superconductors to enter the Fulde–Ferrell–Larkin–Ovchinnikov (FFLO) state [44], it is tempting to attribute these upturns to the appearance of an FFLO state. However, stabilizing an FFLO state in such a dirty superconductor, where ℓ, coherence length ξ, and interparticle distance $(1/k_F)$ are all comparable, is highly nontrivial, as FFLO states typically require a very clean system with $\ell \gg \xi_{ab}$. Our results thus may trigger further studies to explore exotic field-induced superconducting states driven by strong correlation and quantum fluctuations [55].

Finally, we comment on the potential existence of *extended* nematic quantum criticality in FST. The NFL transport in FST is observed over an unexpectedly wide range of x, spanning $0.06 \leqslant x \leqslant 0.45$ [Fig. 4(a)]. This behavior is unusual as it differs from conventional quantum critical metals where NFL behavior is confined to the vicinity of a QCP. One intriguing interpretation of our observation is that the quantum critical regime may be stabilized across the extended parameter range, a phenomenon referred to as *extended* quantum criticality [4]. Although such a behavior has been reported in a few materials, including cuprates [56], heavy fermions [57], magic-angle twisted bilayer graphene [58], and quantum spin-liquids [59,60], it remains rare and, to the best of our knowledge, has not been observed in iron-based superconductors. Further high-field experiments are essential to probe the normal-state transport properties underneath the superconducting dome and determine whether the nematic quantum critical regime extends over a finite parameter range of x in the zero-temperature limit.

In summary, we have investigated the normal-state electrical and thermoelectric transport properties of MBE-grown FST thin films across the pure nematic QCP. In the vicinity of the nematic QCP $x = 0.45$, we find hallmark NFL transport signatures, including T-linear resistivity and logarithmic divergence of S/T, indicating that nematic fluctuations play a key role in driving NFL behavior. Additionally, our estimation of upper critical fields across the nematic QCP reveals a crossover in pair-breaking mechanisms from orbital to Pauli-limited effects with increasing Te content, highlighting the significant impact of nematic criticality-induced mass enhancement on superconducting properties. These findings underscore the profound influence of nematic fluctuations on both normal-state and superconducting behaviors.

We thank N. Nagaosa, Y. Iwasa, S. Kasahara, M. Hirschberger, and R. Yamada for discussions. This work was supported by JSPS KAKENHI Grants No. 24K17020, No. 22K18965, No. 23H04017, No. 23H05431, No. 23H05462, No. 23H04862, No. 24H00417, and No. 24H01652; JST FOREST (Grant No. JPMJFR2038), JST CREST (Grants No. JPMJCR1874 and No. JPMJCR23O3), Mitsubishi Foundation, the special fund of Institute of Industrial Science, the University of Tokyo, the RIKEN TRIP initiative (Many-body Electron Systems), and Sumitomo Foundation.

The data that support the findings of this Letter are available from the authors upon reasonable request.

[1] H. v. Löhneysen, A. Rosch, M. Vojta, and P. Wölfle, Fermi-liquid instabilities at magnetic quantum phase transitions, Rev. Mod. Phys. **79**, 1015 (2007).

[2] T. Shibauchi, A. Carrington, and Y. Matsuda, A quantum critical point lying beneath the superconducting dome in iron pnictides, Annu. Rev. Condens. Matter Phys. **5**, 113 (2014).

[3] S. Paschen and Q. Si, Quantum phases driven by strong correlations, Nat. Rev. Phys. **3**, 9 (2021).

[4] P. W. Phillips, N. E. Hussey, and P. Abbamonte, Stranger than metals, Science **377**, eabh4273 (2022).

[5] Y. Sato, S. Kasahara, H. Murayama, Y. Kasahara, E.-G. Moon, T. Nishizaki, T. Loew, J. Porras, B. Keimer, T. Shibauchi *et al.*, Thermodynamic evidence for a nematic phase transition at the onset of the pseudogap in $YBa_2Cu_3O_y$, Nat. Phys. **13**, 1074 (2017).

[6] R. M. Fernandes, A. I. Coldea, H. Ding, I. R. Fisher, P. Hirschfeld, and G. Kotliar, Iron pnictides and chalcogenides: a new paradigm for superconductivity, Nature (London) **601**, 35 (2022).

[7] L. Nie, K. Sun, W. Ma, D. Song, L. Zheng, Z. Liang, P. Wu, F. Yu, J. Li, M. Shan *et al.*, Charge-density-wave-driven electronic nematicity in a kagome superconductor, Nature (London) **604**, 59 (2022).

[8] Y. Cao, D. Rodan-Legrain, J. M. Park, N. F. Yuan, K. Watanabe, T. Taniguchi, R. M. Fernandes, L. Fu, and P. Jarillo-Herrero, Nematicity and competing orders in superconducting magic-angle graphene, Science **372**, 264 (2021).

[9] B. J. Ramshaw, S. E. Sebastian, R. D. McDonald, J. Day, B. S. Tan, Z. Zhu, J. B. Betts, R. Liang, D. A. Bonn, W. N. Hardy, and N. Harrison, Quasiparticle mass enhancement approaching

optimal doping in a high-T_c superconductor, Science **348**, 317 (2015).

[10] T. Shibauchi, T. Hanaguri, and Y. Matsuda, Exotic superconducting states in FeSe-based materials, J. Phys. Soc. Jpn. **89**, 102002 (2020).

[11] Z. Yin, K. Haule, and G. Kotliar, Kinetic frustration and the nature of the magnetic and paramagnetic states in iron pnictides and iron chalcogenides, Nat. Mater. **10**, 932 (2011).

[12] M. Yi, Y. Zhang, Z.-X. Shen, and D. Lu, Role of the orbital degree of freedom in iron-based superconductors, npj Quantum Mater. **2**, 57 (2017).

[13] K. Mukasa, K. Matsuura, M. Qiu, M. Saito, Y. Sugimura, K. Ishida, M. Otani, Y. Onishi, Y. Mizukami, K. Hashimoto *et al.*, High-pressure phase diagrams of $FeSe_{1-x}Te_x$: Correlation between suppressed nematicity and enhanced superconductivity, Nat. Commun. **12**, 381 (2021).

[14] K. Ishida, Y. Onishi, M. Tsujii, K. Mukasa, M. Qiu, M. Saito, Y. Sugimura, K. Matsuura, Y. Mizukami, K. Hashimoto *et al.*, Pure nematic quantum critical point accompanied by a superconducting dome, Proc. Natl. Acad. Sci. USA **119**, e2110501119 (2022).

[15] Q. Jiang, Y. Shi, M. H. Christensen, J. J. Sanchez, B. Huang, Z. Lin, Z. Liu, P. Malinowski, X. Xu, R. M. Fernandes *et al.*, Nematic fluctuations in an orbital selective superconductor $Fe_{1+y}Te_{1-x}Se_x$, Commun. Phys. **6**, 39 (2023).

[16] W. Bao, Y. Qiu, Q. Huang, M. A. Green, P. Zajdel, M. R. Fitzsimmons, M. Zhernenkov, S. Chang, M. Fang, B. Qian *et al.*, Tunable $(\delta\pi, \delta\pi)$-type antiferromagnetic order in α-Fe(Te,Se) superconductors, Phys. Rev. Lett. **102**, 247001 (2009).

[17] T. Otsuka, S. Hagisawa, Y. Koshika, S. Adachi, T. Usui, N. Sasaki, S. Sasaki, S. Yamaguchi, Y. Nakanishi, M. Yoshizawa *et al.*, Incoherent-coherent crossover and the pseudogap in Te-annealed superconducting $Fe_{1+y}Te_{1-x}Se_x$ revealed by magnetotransport measurements, Phys. Rev. B **99**, 184505 (2019).

[18] Y. Liu, A. Wang, Q. Du, L. Wu, Y. Zhu, and C. Petrovic, Nanoscale inhomogeneity and the evolution of correlation strength in $FeSe_{1-x}S_x$, Nano Convergence **10**, 59 (2023).

[19] S. Licciardello, J. Buhot, J. Lu, J. Ayres, S. Kasahara, Y. Matsuda, T. Shibauchi, and N. Hussey, Electrical resistivity across a nematic quantum critical point, Nature (London) **567**, 213 (2019).

[20] A. I. Coldea, S. F. Blake, S. Kasahara, A. A. Haghighirad, M. D. Watson, W. Knafo, E. S. Choi, A. McCollam, P. Reiss, T. Yamashita *et al.*, Evolution of the low-temperature Fermi surface of superconducting $FeSe_{1-x}S_x$ across a nematic phase transition, npj Quantum Mater. **4**, 2 (2019).

[21] P. Wiecki, K. Rana, A. E. Böhmer, Y. Lee, S. L. Bud'ko, P. C. Canfield, and Y. Furukawa, Persistent correlation between superconductivity and antiferromagnetic fluctuations near a nematic quantum critical point in $FeSe_{1-x}S_x$, Phys. Rev. B **98**, 020507(R) (2018).

[22] D. Arčon, P. Jeglič, A. Zorko, A. Potočnik, A. Y. Ganin, Y. Takabayashi, M. J. Rosseinsky, and K. Prassides, Coexistence of localized and itinerant electronic states in the multiband iron-based superconductor $FeSe_{0.42}Te_{0.58}$, Phys. Rev. B **82**, 140508(R) (2010).

[23] S. Lederer, Y. Schattner, E. Berg, and S. A. Kivelson, Superconductivity and non-Fermi liquid behavior near a nematic quantum critical point, Proc. Natl. Acad. Sci. USA **114**, 4905 (2017).

[24] K. Mukasa, K. Ishida, S. Imajo, M. Qiu, M. Saito, K. Matsuura, Y. Sugimura, S. Liu, Y. Uezono, T. Otsuka *et al.*, Enhanced superconducting pairing strength near a pure nematic quantum critical point, Phys. Rev. X **13**, 011032 (2023).

[25] I. Pallecchi, G. Lamura, M. Tropeano, M. Putti, R. Viennois, E. Giannini, and D. Van der Marel, Seebeck effect in $Fe_{1+x}Te_{1-y}Se_y$ single crystals, Phys. Rev. B **80**, 214511 (2009).

[26] Y. Sun, T. Yamada, S. Pyon, and T. Tamegai, Influence of interstitial Fe to the phase diagram of $Fe_{1+y}Te_{1-x}Se_x$ single crystals, Sci. Rep. **6**, 32290 (2016).

[27] Y. Sato, S. Nagahama, I. Belopolski, R. Yoshimi, M. Kawamura, A. Tsukazaki, N. Kanazawa, K. S. Takahashi, M. Kawasaki, and Y. Tokura, Molecular beam epitaxy of superconducting $FeSe_xTe_{1-x}$ thin films interfaced with magnetic topological insulators, Phys. Rev. Mater. **8**, L041801 (2024).

[28] K. Momma and F. Izumi, VESTA 3 for three-dimensional visualization of crystal, volumetric and morphology data, J. Appl. Crystallogr. **44**, 1272 (2011).

[29] See Supplemental Material at https://link.aps.org/supplemental/10.1103/8zfz-252m for details of sample fabrication, transport and thermoelectricity measurements, and discussions about Kondo effect, MIR limit, and WHH fittings.

[30] W. Li, Y. Zhang, P. Deng, Z. Xu, S.-K. Mo, M. Yi, H. Ding, M. Hashimoto, R. Moore, D.-H. Lu *et al.*, Stripes developed at the strong limit of nematicity in FeSe film, Nat. Phys. **13**, 957 (2017).

[31] Y. Kubota, F. Nabeshima, K. Nakayama, H. Ohsumi, Y. Tanaka, K. Tamasaku, T. Suzuki, K. Okazaki, T. Sato, A. Maeda *et al.*, Pure nematic state in the iron-based superconductor FeSe, Phys. Rev. B **108**, L100501 (2023).

[32] Z. Feng, J. Yuan, G. He, W. Hu, Z. Lin, D. Li, X. Jiang, Y. Huang, S. Ni, J. Li *et al.*, Tunable critical temperature for superconductivity in FeSe thin films by pulsed laser deposition, Sci. Rep. **8**, 4039 (2018).

[33] A. Legros, S. Benhabib, W. Tabis, F. Laliberté, M. Dion, M. Lizaire, B. Vignolle, D. Vignolles, H. Raffy, Z. Li *et al.*, Universal T-linear resistivity and Planckian dissipation in overdoped cuprates, Nat. Phys. **15**, 142 (2019).

[34] I. Paul and G. Kotliar, Thermoelectric behavior near the magnetic quantum critical point, Phys. Rev. B **64**, 184414 (2001).

[35] I. Pallecchi, F. Caglieris, and M. Putti, Thermoelectric properties of iron-based superconductors and parent compounds, Supercond. Sci. Technol. **29**, 073002 (2016).

[36] J. Xu, M. Qin, Z. Lin, X. Zhang, R. Zhang, L. Xu, L. Zhang, Q. Shi, J. Yuan, B. Zhu, C. Dong, R. Xiong, Q. Chen, Y. Li, J. Shi, and K. Jin, *In situ* electrical and thermal transport properties of $Fe_ySe_{1-x}Te_x$ films with ionic liquid gating, Phys. Rev. B **107**, 094514 (2023).

[37] R. Daou, O. Cyr-Choiniere, F. Laliberté, D. LeBoeuf, N. Doiron-Leyraud, J.-Q. Yan, J.-S. Zhou, J. B. Goodenough, and L. Taillefer, Thermopower across the stripe critical point of $La_{1.6-x}Nd_{0.4}Sr_xCuO_4$: Evidence for a quantum critical point in a hole-doped high-T_c superconductor, Phys. Rev. B **79**, 180505(R) (2009).

[38] P. R. Mandal, T. Sarkar, and R. L. Greene, Anomalous quantum criticality in the electron-doped cuprates, Proc. Natl. Acad. Sci. USA **116**, 5991 (2019).

[39] S. Arsenijević, H. Hodovanets, R. Gaál, L. Forró, S. L. Bud'Ko, and P. C. Canfield, Signatures of quantum criticality in the thermopower of $Ba(Fe_{1-x}Co_x)_2As_2$, Phys. Rev. B **87**, 224508 (2013).

[40] H. Mitamura, R. Watanuki, E. Kampert, T. Förster, A. Matsuo, T. Onimaru, N. Onozaki, Y. Amou, K. Wakiya, K. T. Matsumoto, I. Yamamoto, K. Suzuki, S. Zherlitsyn, J. Wosnitza, M. Tokunaga, K. Kindo, and T. Sakakibara, Improved accuracy in high-frequency AC transport measurements in pulsed high magnetic fields, Rev. Sci. Instrum. **91**, 125107 (2020).

[41] K. Behnia, D. Jaccard, and J. Flouquet, On the thermoelectricity of correlated electrons in the zero-temperature limit, J. Phys.: Condens. Matter **16**, 5187 (2004).

[42] Y. Kim, M.-S. Kim, D. Kim, M. Kim, M. Kim, C.-M. Cheng, J. Choi, S. Jung, D. Lu, J. H. Kim *et al.*, Kondo interaction in FeTe and its potential role in the magnetic order, Nat. Commun. **14**, 4145 (2023).

[43] N. R. Werthamer, E. Helfand, and P. C. Hohenberg, Temperature and purity dependence of the superconducting critical field, H_{c2}. III. Electron spin and spin-orbit effects, Phys. Rev. **147**, 295 (1966).

[44] Y. Matsuda and H. Shimahara, Fulde-Ferrell-Larkin-Ovchinnikov state in heavy fermion superconductors, J. Phys. Soc. Jpn. **76**, 051005 (2007).

[45] M. Fang, J. Yang, F. F. Balakirev, Y. Kohama, J. Singleton, B. Qian, Z. Q. Mao, H. Wang, and H. Q. Yuan, Weak anisotropy of the superconducting upper critical field in $Fe_{1.11}Te_{0.6}Se_{0.4}$ single crystals, Phys. Rev. B **81**, 020509(R) (2010).

[46] S. Khim, J. W. Kim, E. S. Choi, Y. Bang, M. Nohara, H. Takagi, and K. H. Kim, Evidence for dominant Pauli paramagnetic effect in the upper critical field of single-crystalline $FeTe_{0.6}Se_{0.4}$, Phys. Rev. B **81**, 184511 (2010).

[47] J. Her, Y. Kohama, Y. Matsuda, K. Kindo, W. Yang, D. Chareev, E. Mitrofanova, O. Volkova, A. Vasiliev, and J.-Y. Lin, Anisotropy in the upper critical field of FeSe and $FeSe_{0.33}Te_{0.67}$ single crystals, Supercond. Sci. Technol. **28**, 045013 (2015).

[48] D. Nakamura, T. Adachi, K. Omori, Y. Koike, and S. Takeyama, Pauli-limit upper critical field of high-temperature superconductor $La_{1.84}Sr_{0.16}CuO_4$, Sci. Rep. **9**, 16949 (2019).

[49] B. Y. Wang, D. Li, B. H. Goodge, K. Lee, M. Osada, S. P. Harvey, L. F. Kourkoutis, M. R. Beasley, and H. Y. Hwang, Isotropic Pauli-limited superconductivity in the infinite-layer nickelate $Nd_{0.775}Sr_{0.225}NiO_2$, Nat. Phys. **17**, 473 (2021).

[50] C. C. Agosta, N. A. Fortune, S. T. Hannahs, S. Gu, L. Liang, J.-H. Park, and J. A. Schleuter, Calorimetric measurements of magnetic-field-induced inhomogeneous superconductivity above the paramagnetic limit, Phys. Rev. Lett. **118**, 267001 (2017).

[51] Y. Cao, V. Fatemi, S. Fang, K. Watanabe, T. Taniguchi, E. Kaxiras, and P. Jarillo-Herrero, Unconventional superconductivity in magic-angle graphene superlattices, Nature (London) **556**, 43 (2018).

[52] P. Wan, O. Zheliuk, N. F. Yuan, X. Peng, L. Zhang, M. Liang, U. Zeitler, S. Wiedmann, N. E. Hussey, T. T. Palstra *et al.*, Orbital Fulde–Ferrell–Larkin–Ovchinnikov state in an Ising superconductor, Nature (London) **619**, 46 (2023).

[53] J. Huang, R. Yu, Z. Xu, J.-X. Zhu, J. S. Oh, Q. Jiang, M. Wang, H. Wu, T. Chen, J. D. Denlinger *et al.*, Correlation-driven electronic reconstruction in $FeTe_{1-x}Se_x$, Commun. Phys. **5**, 29 (2022).

[54] S. Kasahara, T. Watashige, T. Hanaguri, Y. Kohsaka, T. Yamashita, Y. Shimoyama, Y. Mizukami, R. Endo, H. Ikeda, K. Aoyama *et al.*, Field-induced superconducting phase of FeSe in the BCS-BEC cross-over, Proc. Natl. Acad. Sci. USA **111**, 16309 (2014).

[55] S. Kasahara, Y. Sato, S. Licciardello, M. Čulo, S. Arsenijević, T. Ottenbros, T. Tominaga, J. Böker, I. Eremin, T. Shibauchi *et al.*, Evidence for an Fulde-Ferrell-Larkin-Ovchinnikov state with segmented vortices in the BCS-BEC-crossover superconductor FeSe, Phys. Rev. Lett. **124**, 107001 (2020).

[56] K. Jin, N. Butch, K. Kirshenbaum, J. Paglione, and R. Greene, Link between spin fluctuations and electron pairing in copper oxide superconductors, Nature (London) **476**, 73 (2011).

[57] T. Tomita, K. Kuga, Y. Uwatoko, P. Coleman, and S. Nakatsuji, Strange metal without magnetic criticality, Science **349**, 506 (2015).

[58] Y. Cao, D. Chowdhury, D. Rodan-Legrain, O. Rubies-Bigorda, K. Watanabe, T. Taniguchi, T. Senthil, and P. Jarillo-Herrero, Strange metal in magic-angle graphene with near Planckian dissipation, Phys. Rev. Lett. **124**, 076801 (2020).

[59] H. Zhao, J. Zhang, M. Lyu, S. Bachus, Y. Tokiwa, P. Gegenwart, S. Zhang, J. Cheng, Y.-f. Yang, G. Chen *et al.*, Quantum-critical phase from frustrated magnetism in a strongly correlated metal, Nat. Phys. **15**, 1261 (2019).

[60] K. Wakamatsu, Y. Suzuki, T. Fujii, K. Miyagawa, H. Taniguchi, and K. Kanoda, Thermoelectric signature of quantum critical phase in a doped spin-liquid candidate, Nat. Commun. **14**, 3679 (2023).